The role of the synthetic chromophore of GFP in generating polymorphism-dependent on/off photoluminescence

Chantal Carayon, Christiane André-Barrès, Nadine Leygue, Nathalie Merceron-Saffon, Martial Boggio-Pasqua, Suzanne Fery-Forgues

The role of the synthetic chromophore of GFP in generating polymorphism-dependent on/off photoluminescence

Chantal Carayon [a], Christiane André-Barrès [a], Nadine Leygue [a], Nathalie Saffon-Merceron [b], Martial Boggio-Pasqua [c], Suzanne Fery-Forgues [a,*]

[a] *SPCMIB, CNRS UMR5068, Université de Toulouse III Paul Sabatier, 118 route de Narbonne, 31062 Toulouse cedex 9, France*

[b] *Service commun RX, Institut de Chimie de Toulouse, ICT- FR2599, Université de Toulouse III Paul Sabatier, 118 route de Narbonne, 31062 Toulouse cedex 9, France*

[c] *Laboratoire de Chimie et Physique Quantiques (LCPQ), CNRS UMR 5626, Université de Toulouse III Paul Sabatier, 118 route de Narbonne, 31062 Toulouse cedex 9, France*

*Corresponding author. E-mail address: sff@chimie.ups-tlse.fr (S. Fery-Forgues)

ABSTRACT

Polymorphism, i.e. the ability of a solid material to exist in more than one crystal form, gives unique opportunity to study the correlation between the solid-state molecular arrangement and the photoluminescence properties, and allows optimizing the performances of materials with reduced synthesis effort. Compound **1**, which results from the combination of 2-phenylbenzoxazole (PBO) and benzylideneimidazolinone (BDI), was known to be weakly fluorescent in solution and in the solid state. Time-dependent density functional theory (TD-DFT) and spin-flip TD-DFT calculations were first used to revisit the behaviour of the isolated molecule in solution. It was shown that the relaxation pathway in the lowest singlet excited state leads to a thermally-accessible conical intersection (CI), which favours non-radiative deactivation. Then, crystallizing molecule **1** under precise experimental conditions allowed four distinct polymorphs and one solvate to be obtained. Remarkably, forms **1a** and **1b** exhibited strong photoluminescence (PL), while polymorphs **1c-e** were virtually not emissive. Recrystallization allowed passing reversibly from one crystalline species to another. Mechanical stimuli, exhibition to solvent vapours and heating were not very effective, but a non-trivial effect of PL enhancement upon freezing was observed for **1a** and **1b**. The non-emissive polymorphs were characterized by the presence of a centrosymmetric dimer

structured by hydrogen bonds, in which paired molecules vibrate with the same mode and are in turn subjected to maximum deformation, according to DFT calculations. Based on the whole set of results, possible deactivation mechanisms were proposed to account for the opposite PL behaviour of the two types of crystalline species. It is shown that the emergence of polymorphism and of a rare on/off PL mechanism may be attributed to the presence of the BDI unit in the molecule.

1. Introduction

Organic crystalline materials that exhibit tunable and switchable photoluminescence (PL) emission find promising applications in the fields of sensors, data storage and optoelectronic devices [1,2]. There is considerable research interest in controlling their optical properties through non-covalent routes, by modulating molecular conformation, as well as the collective arrangement and interaction mode of molecules in the solid [3−5]. The smartest way to achieve this goal is probably to take advantage of polymorphism, i.e. the ability of a solid material to exist in more than one crystal form [6−9]. Since this approach considers exactly the same molecule, it gives unique opportunity to make precise structure-property correlations, and leads to optimized performances of materials with reduced synthesis effort. Moreover, as polymorphs generally differ by a small amount of energy, the transition between them may be easily achieved under ambient conditions, and this opens the door to stimuli-responsive materials and their applications [4,5,9−11]. There are many examples of polymorphs that exhibit very different emission colour and intensity [11−19] while total or almost total on/off switching of emission has rarely been reported [20−26].

Over the last few years, our group introduced new molecules [27,28] resulting from the combination of 2-phenylbenzoxazole (PBO) [29] and benzylideneimidazolinone (BDI), i.e. a synthetic derivative of the chromophore of the well-known Green Fluorescent Protein [30] (Fig. S1). All these molecules had the same electron conjugated system and were weakly fluorescent in organic solutions. Those bearing an alkyl chain (from C4 to C16) on the BDI nitrogen atom showed strong aggregation-induced emission enhancement (AIEE) effect, [31] and were good solid-state emitters. Curiously, the first member of the series bearing a methyl group (**1**, Fig. 1) was almost not emissive in the aggregated and solid states. This discrepancy prompted us to undertake the present work. First, the photophysical mechanism that explains

the weak fluorescence in solution was revisited using spin-flip time-dependent density functional theory (SF-TD-DFT) and TD-DFT calculations. Then, it was shown that not only compound **1** exists as many polymorph forms, an unprecedented case for PBO derivatives, but polymorphism controls on/off solid-state PL. In conjunction with the results of IR spectroscopy and various quantum chemical calculations, an original mechanism was proposed to rationalize these data, and to explain how the presence of the BDI unit endows the molecules with this exceptional behaviour.

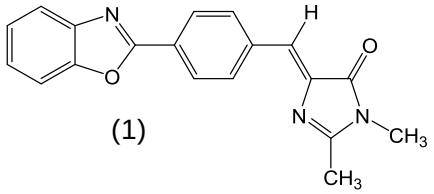

(1)

Fig. 1. Chemical structure of compound **1**.

2. Experimental section

2.1. Materials and methods

Methanol (HPLC grade) and petroleum ether (reagent grade) were from Fisher Chemicals. Chromasolv HPLC grade dichloromethane and *n*-heptane, and reagent grade chloroform, were from Sigma-Aldrich. HPLC grade acetonitrile and analytical grade THF were from SDS. All solvents were used without further purification.

Compound **1** was synthesized as previously described [27] and purified on silica column chromatography using petroleum ether/CH_2Cl_2 as eluent, resulting in yellow microcrystalline powder. Purity was checked by thin layer chromatography. Single crystals were grown by dissolving an aliquot (3 mg) of the pristine powder in an organic solvent with gentle heating, and then evaporating the solvent in conditions indicated in Table S1.

2.2. Apparatus

The melting points were measured on a Stuart Automatic SMP40 apparatus. The photoluminescence spectra were recorded using a Xenius SAFAS spectrofluorimeter equipped with a $BaSO_4$ integrating sphere. They were corrected using a home-made

correction curve. Low temperature measurements were done on powder samples dispersed in KBr. For the measurement of quantum yields, the excitation source was scanned in order to evaluate the reflected light for the empty sphere (L_a), the samples facing the source light (L_c) and the sample out of the irradiation beam (L_b). The luminescence spectra were recorded with the sample facing the source light (E_c) and out from direct irradiation (E_b). The PM voltage was adapted to the measurement of reflected light and emission spectra, respectively, and proper correction was applied to take into account the voltage difference. The absolute photoluminescence quantum yield values (Φ_{PL}) were calculated by a method based on the one developed by de Mello *et al.* [32] using the formula:

$$\Phi_{PL} = [E_c\text{-}(1\text{-}\alpha)E_b]/L_a\alpha \quad (1)$$

with $\alpha = 1\text{-}L_c/L_b$. The error on the Φ_{PL} value was estimated to be about 20%. Fourier transform infrared (FTIR) spectra were recorded using a Nexus ThermoNicolet FTIR spectrophotometer equipped with a diamond ATR.

2.3. Crystallography

Crystal data were collected at 193(2)K (**1b**, **1c** and **1d**) and 293(2)K (**1e**) on a Bruker-AXS APEX II diffractometer equipped with a 30 W air-cooled microfocus source (ImS) with focusing multilayer optics (**1b**, **1c** and **1d**) and on a Bruker-AXS D8-Venture diffractometer equipped with a CMOS detector (photon100), using MoKα radiation (λ = 0.71073 Å). The structures were solved using an intrinsic phasing method (ShelXT) [33]. All non-hydrogen atoms were refined anisotropically using the least-squares method on F^2 [34]. Molecular graphics were generated using the program MERCURY [35]. Molecular views and crystal data of all polymorphs are given in Fig. S2 and Table S2, respectively. CCDC supplementary crystallographic data can be obtained free of charge from The Cambridge Crystallographic Data Centre via https://www.ccdc.cam.ac.uk/structures.

The X-ray powder diffraction patterns were recorded in the "Nano X platform of CEMES-CNRS". The powders were placed in a sample holder with no background noise. The measurements were made in reflection mode using a Bragg-Brentano configuration on a Bruker D8 Advance diffractometer equipped with a Copper anticathode (Cu Kα1 = 1.54059 Å and Kα2 = 1.54439 Å) and a 1D Lynx eye detector.

2.4. DFT, TD-DFT and SF-TD-DFT calculations

DFT calculations of the harmonic normal modes were performed at the B3LYP/6-31+G(d,p) level of theory [36] for dimers **1a**, **1b**, **1c**, **1d**, **1e** obtained from X-ray data (Table S5). The frequencies were calculated using a scaling factor of 0.9613 [37]. The ground- and first excited-state potential energy surfaces of a model isolated monomer were explored at the TD-DFT and SF-TD-DFT levels of theory. TD-DFT and SF-TD-DFT calculations were performed with the PBE0 [38] functional and BH&HLYP [39] functionals, respectively, and the 6-31+G(d,p) basis set. The SF-TD-DFT calculations used a reference triplet state obtained from a restricted open-shell DFT calculation. The excited-state transition state was optimized at the TD-DFT level only, for which analytical second derivatives of the energy with respect to nuclear coordinates could be computed. On the other hand, the twisted minimum and conical intersection could only be optimized with SF-TD-DFT, which allows a correct description of the potential energy surface topology where the ground- and first excited state couple [40]. DFT and TD-DFT calculations were performed with Gaussian [41] and Gamess [42] quantum chemistry codes, respectively. The geometries (Cartesian coordinates) of optimized structures obtained at TD-DFT and SF-TD-DFT levels are given in Table S6.

3. Results and discussion

3.1. Revisiting the spectroscopic behaviour in solution: Spin-flip TD-DFT calculations

It was shown in our previous work that all compounds of this series emit weak blue light in organic solvents (e.g. λ_{em}^{max} = 448 nm, Φ_F = 0.02 for **1** in ethanol) [27]. To explain this behaviour, it was proposed that the two molecular moieties that rotate around the vinylene link lead to dispersion of the excitation energy. The PL enhancement observed for the long-chain analogues was classically attributed to rigidification of the molecular backbone and restriction of internal rotations [31]. However, regarding recent findings in this research field [43,44], it seemed necessary to us to better understand what happens in solutions. To do so, time-dependent density functional theory (TD-DFT) and its spin-flip variant (SF-TD-DFT), which allows the correct description of conical intersections (CIs) between ground and excited states [45], were used to investigate the lowest singlet excited state (S_1) relaxation pathway by first considering an isolated model system *in vacuum*. The model system was built by replacing the two methyl groups of the imidazolinone moiety by hydrogen atoms.

Fig. 2 shows that upon excitation to the S_1 state, the system first relaxes to a planar structure (Min-S_1-planar) which is assigned to the emissive species. The calculated emission

wavelength at the TD-DFT level (435 nm) is consistent with that observed in solution. This structure is characterized by a slight shortening of 0.03 Å of the C–C bond between the benzoxazole and BDI moieties, a more substantial shortening of 0.06 Å of the phenyl-bridge C–C bond length and a lengthening of 0.06 Å of the imidazolinone-bridge C–C bond length. However, this minimum is not the lowest energy excited-state structure on the S_1 potential energy surface. Along the torsion coordinate of the imidazolinone moiety, a lower energy S_1 minimum (Min-S_1-Im-twist) can be found in which the torsion dihedral angle of the imidazolinone moiety is 94° with respect to the rest of the molecule. A slight pyramidalization (ca. 5°) of the carbon atom linked to the bridge is also involved. This global minimum on the S_1 potential energy surface is located 6.5 kcal/mol below the S_1 planar minimum, and can be reached by overcoming a small excited-state potential energy barrier of about 6 kcal/mol from Min-S_1-planar. Interestingly, upon further imidazolinone torsion to 102° and pyramidalization of the imidazolinone carbon atom linked to the bridge to 50°, a low-lying S_0/S_1 minimum energy conical intersection (S_0/S_1-$MECI_{Im\text{-}twist}$) is reached requiring only an activation energy of 8.5 kcal/mol from Min-S_1-Im-twist. This CI is located at a similar energy to the S_1 planar minimum and below the Franck-Condon region. This is reminiscent of the potential energy surface topology found in the neutral green fluorescent protein chromophore belonging to the BDI family [46]. This CI, *i.e.* a critical structure of the potential energy surfaces where the S_1 and S_0 states are degenerate and the probability of non-radiative internal conversion is most efficient [29], is most likely responsible for the very efficient non-radiative decay of **1** in solution, where molecules can move freely.

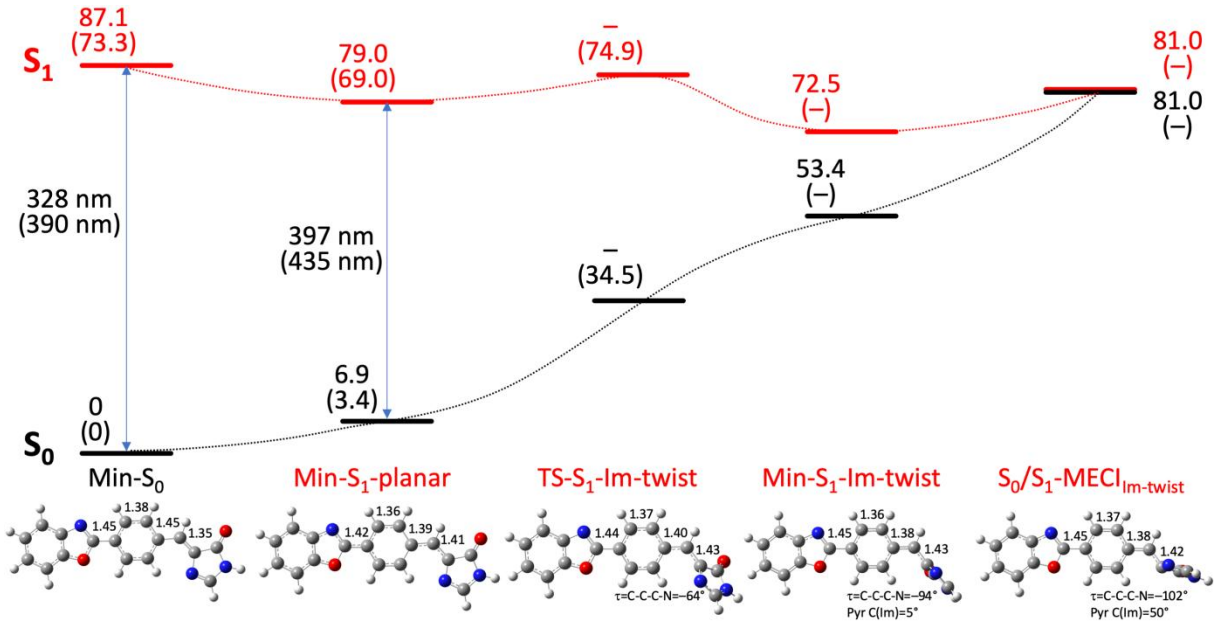

Fig. 2. Schematic potential energy profile for the isolated model molecule of **1** along the main S_1 excited-state relaxation pathway. Energies are in kcal/mol with respect to the ground-state minimum (Min-S_0). SF-TD-DFT values are in normal font and TD-DFT values are in parentheses. Geometries are obtained at SF-TD-DFT level, except for TS-S_1-Im-twist (optimized with TD-DFT). Relevant bond lengths (Å) and angles for torsion and pyramidalization are shown.

3.2. Preparation and characterization of the various crystalline forms

To study the properties of **1** in the solid state, this compound was synthesized according to a variant of our previously described procedure and single crystals suitable for X-ray analysis were grown by evaporation of organic solutions under various experimental conditions (Table S1). In some cases, two types of crystals co-existed and were sorted manually. The X-ray analysis led to identification of one acetonitrile solvate (**1b**) and four polymorphs (**1a, 1c-e**) including one previously reported structure [27]. It is obvious that not only the solvent, but also the temperature and speed of solvent evaporation, played a key role in the preparation of these various crystalline forms. Regarding outward appearance, the crystals were roughly divided into two groups. Forms **1a** and **1b** had needle or rod-like shapes, the other ones (**1c-e**) were irregular plates of varying thickness (Fig. 3). The crystal colour ranged from pale yellow to yellow-orange. The melting points were between 214.7 and 216.0 °C, with one exception (207.4°C) for solvate **1b**. The very close energy levels explain

the formation of concomitant polymorphs and the easy transition from one form to another that was observed in the course of the preparation of crystals.

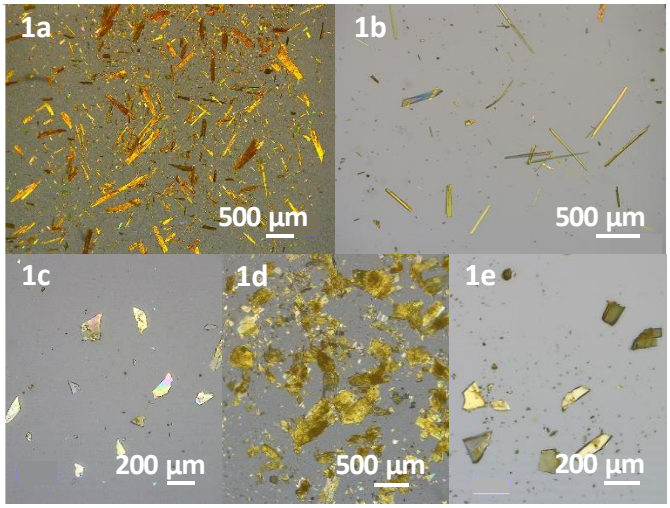

Fig. 3. Optical microscopy images of solvate **1b** and polymorphs **1a**, **1c**, **1d** and **1e**.

The examination of the X-ray structures provides a lot of precious information on the geometry of molecules and mutual interactions between them. Crystallographic data are collected in Table S2 and molecular structures are given in Fig. S2. The inversion between oxazole N and O atoms is frequently found in crystallographic structures of PBO [29]. In the present case, this trend and the dissymmetry brought by the BDI unit lead to the emergence of two conformers, named *syn* and *anti* depending on the relative position of the benzoxazole and imidazolinone oxygen atoms on the same side or on the opposite side with respect to the long axis of the molecule (Fig. S3). For instance, crystals of **1d** (and possibly **1a** and **1c**) contained only molecules in the *anti* conformation, while **1b** and **1e** contained more than 80% of molecules in the *syn* conformation.

Molecules were almost planar in solvate **1b**, where packing forces are weak, and in **1a**. They were moderately twisted in polymorphs **1c-e**, with the benzoxazole and imidazolinone moieties forming a dihedral angle below or equal to 20° (Table S3). It must be underlined that this twist is distributed over the entire molecular structure, and not localized between two adjacent aromatic rings. If the relative position of the oxazole N and O atom is not considered, the superimposition of all molecules reveals that other geometrical changes are not very significant (Fig. S4). Two types of molecular arrangements can be distinguished as illustrated in Fig. 4. In crystals of **1a** and **1b**, molecules showed a crossed arrangement, typical of many PBO derivatives [29]. In the other crystals, molecules were aligned along their long axis, with

the PBO moieties situated in parallel (**1c** and **1e)** or slightly different planes (**1d**). In every case, the nearest neighbours were distant by ~3.3 Å in the stacking direction, and were anti-parallel to each other. Several π-π interactions were detected for every crystalline form (see Table S3 and Fig. 5). Noticeably, the overlap of the aromatic moieties was pronounced for **1a**, slightly weaker for **1b**. The strongest π-π interactions are between the benzoxazole ring of one molecule and the imidazolinone ring of a neighbouring molecule in the stacking direction. In contrast, no or very weak overlap of the aromatic moieties was observed for **1c**-**e**, due to slippage of molecules in the long molecular axis direction (Fig. S5), and π-π interactions take place between two imidazolinone rings. At least one CH-π interaction involving one hydrogen atom borne by the methyl group of the imidazolinone cycle and a 6-membered ring can also be found for each crystalline species. Regarding hydrogen bonds between 2.4 and 2.8 Å (Table S4), the only commonality between all crystals is the involvement of the imidazolinone oxygen atom in an intermolecular H-bond that strongly structures the network. In **1a** and **1b**, this bond is directed towards one hydrogen atom of the benzoxazole moiety of the neighboring molecule, leading to a compact arrangement. In contrast, for **1c**-**e**, the H-bond involves the hydrogen atoms of the phenyl and vinyl groups, so that molecules form sort of centrosymmetric dimers. The overall result is that the BDI moieties of the molecules seem to be tightly bound as columns, while the benzoxazole moieties have a looser environment. Other types of short contacts were encountered, or not, in the various structures, involving for example the oxazole nitrogen and oxygen atoms.

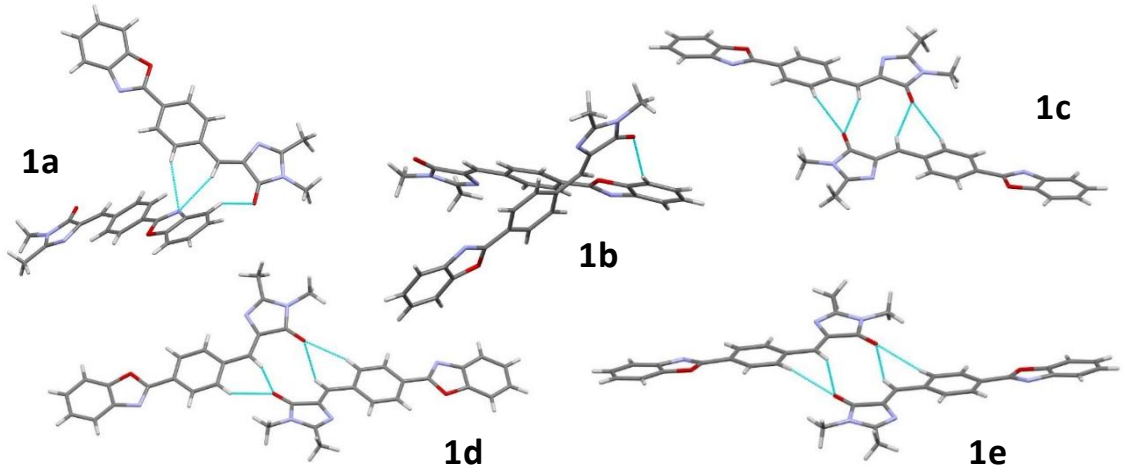

Fig. 4. Molecular arrangement of the five crystalline forms of **1**, showing the short contacts that involve the imidazolinone oxygen atom (blue ink).

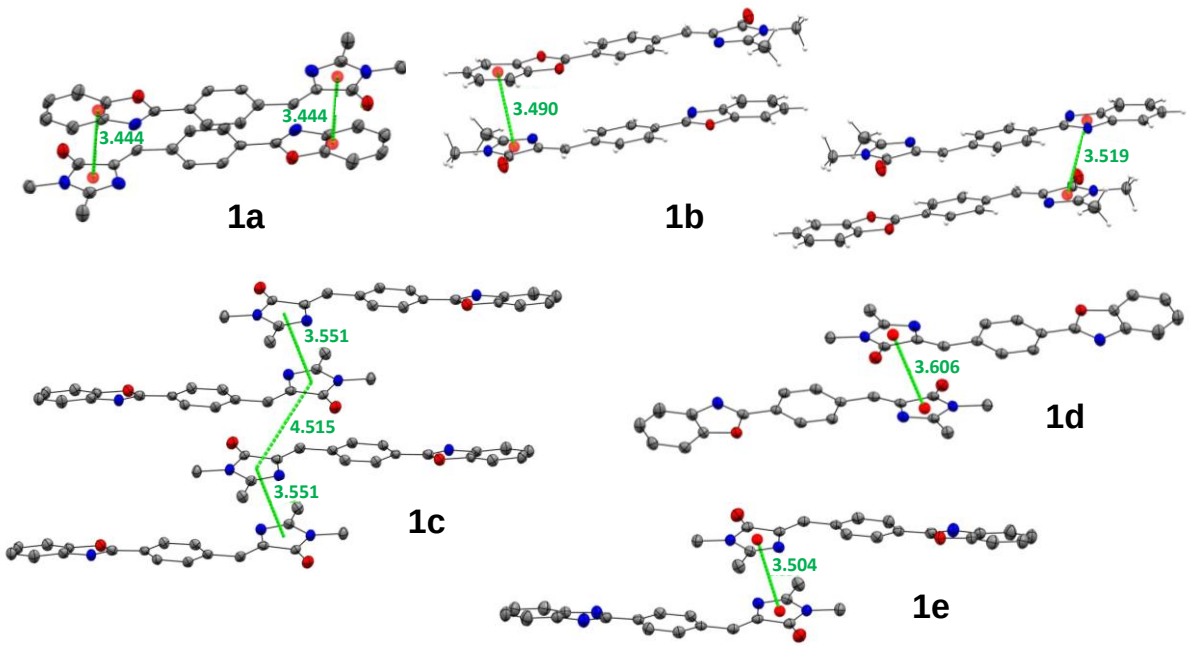

Fig. 5. Molecular views showing π-π interactions for the five crystalline forms of **1**. Distances in Å.

3.3. Infrared spectroscopy and DFT calculations

To examine the H-bonds formed by the imidazolinone oxygen atom in greater detail, the FTIR spectra of the five crystalline species were recorded. The peaks corresponding to the C=O stretching vibrations were situated around 1701 cm^{-1} for **1a** and **1b**, and around 1707 cm^{-1} for **1c-e** (Fig. S7). As the same molecule is considered, these results suggest that the order of the covalent bond is weaker, and hence the H-bond is stronger, for **1a** and **1b** than for **1c-e**. At lower frequencies, in the fingerprint region, peaks were at 749 and 733 cm^{-1}, respectively (Fig. S8). They seem to indicate that deformations of C-H bonds were stronger in **1c-e** than in **1a** and **1b.** The differences between the frequency values are small, but it is clear that the two types of crystals have a distinct IR signature.

To get a deeper insight, DFT frequency analyses were first performed on the HBDI unit in the gas phase used as reference, and then on the five crystalline species (Table S5). Adjacent molecules linked by H-bonds involving the C=O(imid) group were considered in each case on the basis of X-ray data. The choice was made to keep the constraints imposed by the crystal packing, instead of calculating the equilibrium geometries, which do not reflect what is actually taking place in the crystals. In this case, the calculation of harmonic

frequencies is not exact. Consequently, the results collected in Table 1 must be considered with some caution, but we think that they provide precious elements of comparison between the crystalline species. For the centrosymmetric dimers of **1c**, **1d** and **1e**, the H-bonds formed between the two C=O(imid) and either H-C(phen) or H-C(vinyl) were examined. Remarkably, for every calculated frequency, two very close values were found, respectively associated with very high and near-zero intensity. This indicates that the normal modes of vibration are degenerated, the two molecules vibrating together with the same mode. A consequence is the dramatic overall deformation of the dimer, the two molecules of which undergo maximal deformation alternately. In contrast, for **1a** and **1b**, each C=O(imid) group presented its own stretching vibration of moderate intensity. Therefore, molecular deformation was weak, as for HBDI in the gas phase. Films showing the stretching vibrations of carbonyl groups, and related molecular deformations, are consigned as supplementary data. Calculations suggest that the associated intensities play a far more important role than the actual frequency values. These data are not accessible experimentally, because they are hidden by the envelope of IR spectra, as shown by the calculated IR spectra (Fig. S10).

Table 1

Calculated C=O(imid)···H-C frequencies in cm^{-1} with a scaled factor of 0.9613, and associated intensities between brackets.

Compound	**HBDI**	**1a**	**1b**	**1c**	**1d**	**1e**
$\nu_{(C=O\cdots H-C)}$ in cm^{-1} (Intensity)	1707(455)	1657(541) 1710 (411)	1762 (729) 1756 (372)	1759 (1626) 1754 (0.00)	1710 (1210) 1707 (0.24)	1773 (1522) 1768 (0.00)

3.4. Spectroscopic properties

The microcrystalline powder of **1a** appeared to be strongly emissive in the green region, with maximum near 502 nm and photoluminescence quantum yield of 0.22 (Fig. 6). Agglomerates of microcrystals had a slightly more yellow emission, probably due to reabsorption effects [47]. With aging, the sample exhibited a shoulder near 550 nm (Fig. 7b), but no distinct crystalline species could be characterized. Solvate **1b** emitted in the yellow-orange region (582 nm), with a weaker but still significant quantum yield (0.11). The differences observed between the emission properties of **1a** and **1b** can be explained as follows. The sharp green emission of **1a** could be assigned to excitons [48,49] or individual

molecules that interact with each other in the crystalline environment [50], while the broad long-wavelength emission of **1b** suggests the additional contribution of excimers as previously proposed for the long chain analogues [27]. At the opposite, polymorph **1d** was very weakly emissive, and **1c** and **1e** were virtually not emissive.

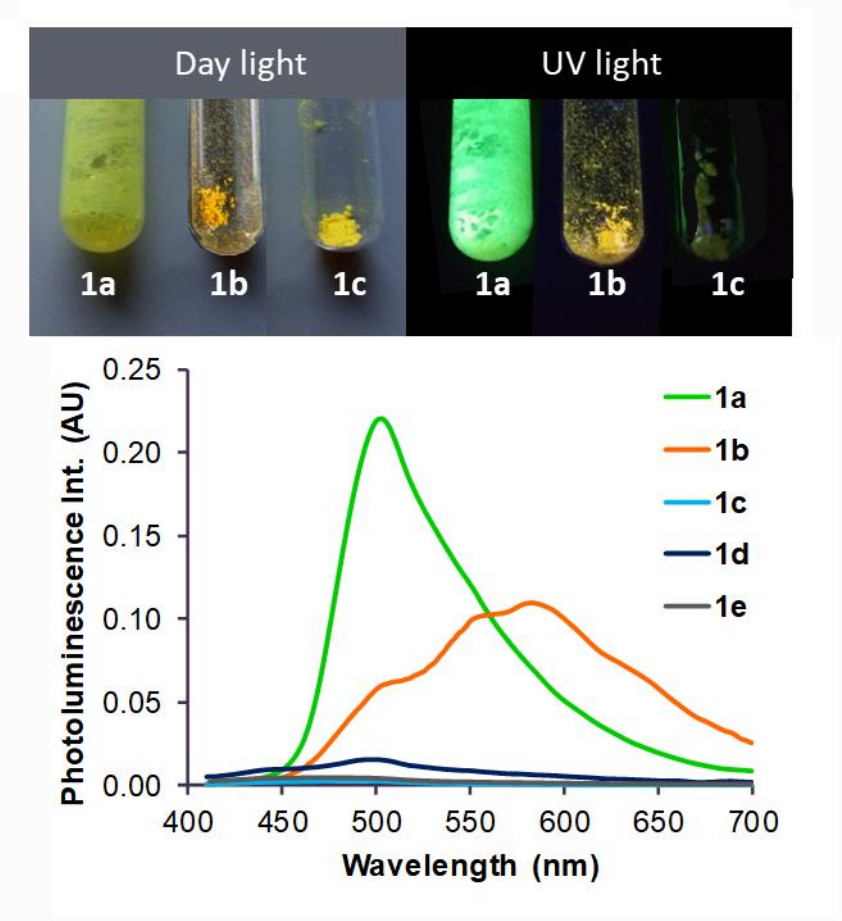

Fig. 6. Top: Photographs of microcrystalline powders of **1a, 1b** and **1c** illuminated by day light and UV light (365 nm). Bottom: PL spectra of the five crystalline forms. λ_{ex} = 380 nm, maximum intensity proportional to quantum yield.

Passing from **1a** and **1b** to **1c-e** by recrystallization in appropriate solvent, and *vice versa*, resulted in turning photoluminescence on and off. The process was reversible many times, although the non-emissive polymorphs were more and more difficult to obtain over time, probably due to their lower stability and to the unavoidable presence of germs of the emissive polymorphs in the laboratory [51]. Other methods of switching from one crystalline form to another have been tried. Upon grinding, the shape of the PL spectrum of **1a** was unchanged. In contrast, the PL spectrum of **1b** was shifted to the blue till 500 nm. Exposition of the ground powder to acetonitrile vapours during 48 h led to a marked decrease of intensity, accompanied by a broadening of the PL spectrum due to the appearance of a band in

the orange region (Fig. S9). This partially reversible mechanofluorochromic effect was rather attributed to amorphization of the sample and then to partial restoration of the crystalline structure due to solvent vapours. Grinding also led to the appearance of a weak PL signal for the non-emissive polymorphs, which rapidly faded when the sample was left to stand alone at room temperature. Efforts were not pursued in this direction because the effects were not strong enough to be harnessed. Finally, heating samples of **1a** and **1d** at 90°C for 24 h did not alter their emission properties, suggesting that this temperature rise did not allow interconversion between polymorphs.

However, an interesting effect was noticed when studying the behaviour of our compounds at various temperatures. In fact, dropping a flask of **1a** into liquid nitrogen resulted in a sharp increase of PL, without noticeable change of the initial colour (Fig. 7a). Since our fluorimeter did not allow controlling the temperature of solid samples, measurements started when the sample was just removed from the liquid nitrogen, and continued when progressively returning to room temperature. In these conditions, the maximum PL intensity recorded for the samples at low temperature (LT) was 3.2 times more intense than at room temperature, and this difference would probably be greater if the sample could be maintained at -196 °C. The intensity change was consistent during many thermal cycles (Fig. 7b). No alteration of the spectrum shape was observed (Fig. 7c), indicating that there is no change in the crystal structure (i.e. crystal packing release followed by large structural relaxation [52,53] or interconversion of polymorph forms by heating and cooling [54,55]) or photophysical processes [56,57] with changing temperature. Very close results were obtained for **1b**, with the difference that the long-wavelength region of the spectrum was narrower for the frozen sample than at room temperature. In contrast, no significant PL enhancement was detected at low temperature for samples of **1c**-**e**.

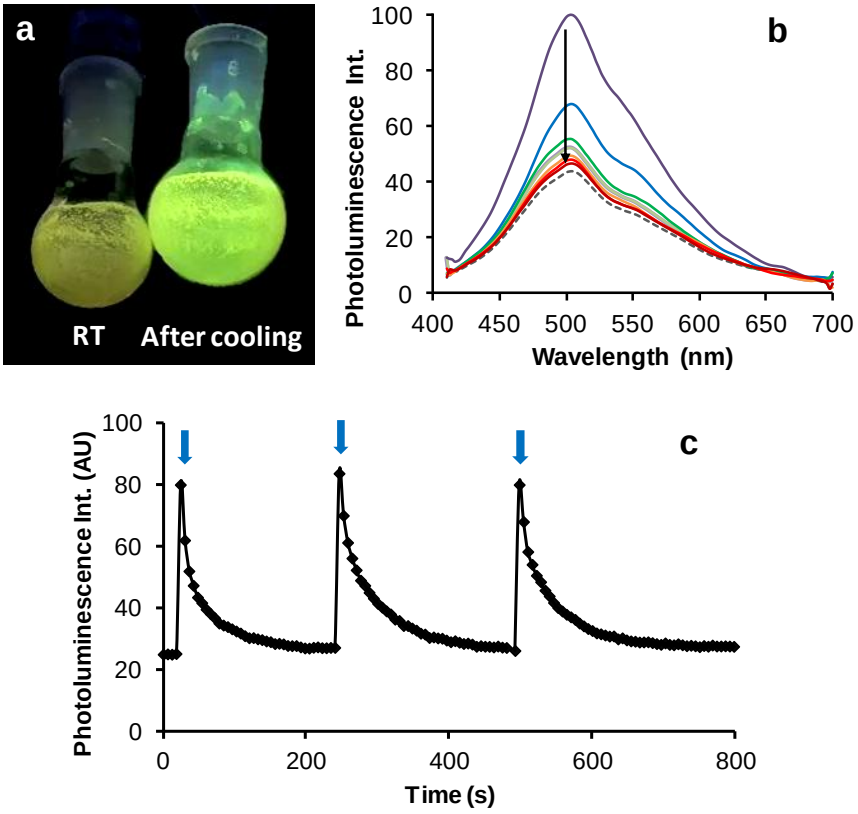

Fig. 7. a) Comparative emission of microcrystalline powder **1a** illuminated by UV light (365 nm) at room temperature and after cooling in liquid nitrogen. b) Variation of the PL spectrum just after cooling (purple line) and during progressive return to room temperature (one spectrum every 50 s). The arrow indicates the sense of the variation. The dashed line corresponds to the initial spectrum recorded at 20°C. c) Variation of the emission intensity just after cooling the sample (arrows) and during progressive return to room temperature (λ_{ex} = 380 nm, λ_{em} = 550 nm).

3.5. Towards an understanding of the contrasting solid-state spectroscopic behaviour

The chemical structure of molecule **1** was unchanged in the various crystalline samples, which nevertheless can be divided in two groups with opposite emission behaviours. Explaining the emission of **1a** and **1b** by evoking the restriction of molecular motions in the solid state is obviously insufficient, because rigidification also occurs for the non-emissive species. The origin of the spectroscopic variations must be sought in the crystal structure. Obviously, the emission properties do not depend on the *syn* or *anti* molecular conformation. The planarity of **1a** and **1b** was a good indication for PL, but the twist observed for **1c-e** is not

enough to account for the extinction of luminescence. In fact, the butyl and hexadecyl analogues of **1** have dihedral angles close to 14° and 31° (Fig. S6), respectively, and are very emissive in the solid state [27,28].

It was shown above that the presence of a thermally-accessible conical intersection is probably responsible for the non-radiative release of excitation energy of the molecule in solution. It is reasonable to assume that it also opens the main non-radiative deactivation pathway of **1** in the solid state. The CI may be located at higher energies due to steric constraints in solids, impeding the non-radiative deactivation pathway and enhancing the PL emission with respect to solutions. This restricted access to conical intersection (RACI) is now recognized for underlying the behaviour of numerous SLE-active molecules [44]. To explain why the two types of polymorphs have such a different behaviour, it is tempting to say that the CI is higher in energy and thus less accessible in **1a** and **1b** than in **1c-e**. Optimizing the CI structures and finding their energy position in the different polymorphs are beyond the aim of this work, although sophisticated computational strategies have been proposed to take the crystal environment into account in such calculations [58]. Here, we will simply use qualitative arguments to consider the possibility of molecular motions within the crystals to provide some clues as to whether the CI is accessible or not.

In **1a** and **1b**, the overlap of the aromatic moieties is significant and π-π interactions take place at short distances. The π-π stacking and the strong packing due to short contacts limit molecular motions [26], so that rotation is impeded and the CI becomes inaccessible. Only the relaxation pathway leading to the planar minimum Min-S_1-planar responsible for PL would be available for molecules situated in the crystal bulk, thus explaining the strong PL of these samples. Moreover, in the present case, the molecules situated at the crystal surface could have more freedom to rotate, and act as PL traps. This would be in line with the observations made at low temperature. Indeed, the PL increase observed at LT most probably arises from the reduced rate of thermally-activated processes, which encompass molecular motions [49,59–61], as well as exciton migration and quenching by non-emissive surface defects [62]. For solvate **1b**, the narrowing of the long-wavelength region of the spectrum of the frozen sample also suggests the involvement of excimers, whose emission can be reduced at LT [63].

For **1c-e**, at first glance, the BDI units seem to be quite rigid in the crystals due to both stacking of the imidazolinone moiety and formation of the centrosymmetric dimers. However, the BDI units are stacked between one another, whereas in **1a-b**, they are facing the benzoxazole units. This would possibly allow for a concerted torsion of the imidazolinone

moieties allowing access to the CI in the solid state. Another option would be that the CIs involved in the non-radiative decay process in the aggregate phase of **1c-e** are different from that computed for the isolated monomer. The steric constraints imposed by the crystal environment may forbid the access to the fairly large amplitude motion necessary to reach S_0/S_1-$MECI_{Im\text{-}twist}$, and could possibly involve a more volume-conserving motion, as observed for example in some acenimides [44].

Finally, another possibility is that the extinction of PL is correlated with the presence of several hydrogen bonds. Assuming that the deformations observed for **1c**, **1d** and **1e** in the ground state also take place in the excited state, they could be partly responsible for the extinction of PL via dispersion of the excitation energy along the C=O···H–C vibrations. It can be noticed that total PL extinction was observed for samples **1c** and **1e**, where deformation is the strongest. Such a deactivation pathway would be particularly original because H-bonds are generally considered to rigidify the molecular structures and activate the SLE processes of numerous fluorophores [64−67], although the opposite behaviour was recently reported by us for hydroxy-substituted PBO derivatives [68]. Clearly, dimeric structures like the ones studied in the present work would deserve more attention regarding their solid-state photophysical properties.

4. Conclusion

In conclusion, five distinct crystalline forms were identified for the same PBO derivative, which is unprecedented, and a rare on/off fluorescence switching effect was reported. In the literature, non-emissive polymorphs of a solid-state fluorescent compound result from a molecular twist [20−23], or from a detrimental packing mode, including edge-to-face interactions [26] or face-to-face π-π stacking [23−25]. To the best of our knowledge, the involvement of CI was proposed here for the first time.

Obviously, both polymorphism and PL switching are related to the presence of the small BDI unit, which is also responsible for the SLE behavior of compound **1**. It is now important to check whether the BDI moiety may confer this set of properties to other types of molecules, which would make it a precious “polymorphogenic” building block. In addition to their interest for practical applications, such BDI derivatives would be ideal tools for exploring the link between molecular arrangement, vibrational modes and excited states in photoluminescent organic crystals.

Furthermore, a fast screening with more than 30 commercially-available dyes in the solid state indicated that PL enhancement at LT is a non-trivial process, which was only observed for one sixth of the investigated dyes (i.e. Pyrene, Coumarin 6, Coumarin 153, Rhodamin B, DCM). Remarkably, no significant PL enhancement at LT was detected for dyes that do not emit at room temperature. It could be instructive to know what these dyes have in common with compound **1**, from a photophysical point of view. This could enable further developments towards new thermochromic materials.

Acknowledgements

ANR is gratefully acknowledged for funding (SUPERFON project # ANR-17-CE07-0029-03). We are indebted to Mr. Nicolas Ratel-Ramond (CEMES-CNRS) for the measurement of XRPD patterns, Ms. Grace Bauger for help in synthesis and Dr. Corinne Routaboul (Service commun IR, ICT) for FTIR spectra.

Electronic supplementary data

Conditions for the preparation of the various crystalline forms, physico-chemical characteristics, crystallographic data, molecular views, optical microscopy images, IR spectra, DFT calculations of the H-bond frequencies and videos showing molecular deformations. CCDC: 1997405, 1997406, 1997407, 1997408.

Keywords

Photoluminescence; Polymorphism; Organic Crystal; Green Fluorescent Protein; Conical intersection

References

[1] Zhang JN, Kang H, Li N, Zhou SM, Sun HM, Yin SW, Zhao N, Tang BZ. Organic solid fluorophores regulated by subtle structure modification: color-tunable and aggregation-induced emission. *Chem. Sci.* **2017**;*8*:577−582. DOI: 10.1039/C6SC02875F

[2] Yang W, Liu C, Lu S, Du J, Gao Q, Zhang R, Liu Y, Yang C. Smart On-Off Switching Luminescence Materials with Reversible Piezochromism and Basichromism. *ChemistrySelect* **2017**; *2*:9215−9221. DOI: 10.1002/slct.201701997

[3] Anthony SP. Organic Solid-State Fluorescence: Strategies for Generating Switchable and Tunable Fluorescent Materials. *ChemPlusChem* **2012**;*77*:518−531. DOI: 10.1002/cplu.201200073

[4] Varughese S. Non-covalent routes to tune the optical properties of molecular materials. *J. Mater. Chem. C* **2014**;*2*:3499–3516. DOI: 10.1039/C3TC32414A

[5] Wang C, Li Z. Molecular conformation and packing: their critical roles in the emission performance of mechanochromic fluorescence materials. *Mater. Chem. Front.* **2017**;*1*:2174–2194. https://doi.org/10.1039/C7QM00201G

[6] Lu B, Liu S, Yan D. Recent advances in photofunctional polymorphs of molecular materials. *Chin. Chem. Lett.* **2019**;*30*:1908–1922. DOI: 10.1016/j.cclet.2019.09.012

[7] Tan R, Wang S, Lan H, Xiao S. Polymorphism-Dependent and Mechanochromic Luminescent Molecules. *Curr. Org. Chem.* **2017**;*21*:236–248. DOI: 10.2174/1385272820666160905104014

[8] Nangia A. Conformational Polymorphism in Organic Crystals. *Acc. Chem. Res.* **2008**;*41*:595−604. DOI:10.1021/ar700203k

[9] Yan D, Evans DG. Molecular crystalline materials with tunable luminescent properties: from polymorphs to multi-component solids. *Mater. Horiz.* **2014**;*1*:46–57. DOI: 10.1039/C3MH00023K

[10] Ma Z, Wang Z, Teng M, Xu Z, Jia X. Mechanically Induced Multicolor Change of Luminescent Materials. *ChemPhysChem* **2015**, *16*, 1811–1828. DOI: 10.1002/cphc.201500181

[11] Du X, Xu F, Yuan M-S, Xue P, Zhao L, Wang D-E, Wang W, Tu Q, Chen S-W, Wang J. Reversible luminescence color switching in the crystal polymorphs of 2,7-bis(2′-methyl-[1,1′-biphenyl]-4-yl)-fluorenone by thermal and mechanical stimuli. *J. Mater. Chem. C* **2016**;*4*:8724–8730. DOI: 10.1039/C6TC02804G

[12] Yoon S-J, Park SY. Polymorphic and mechanochromic luminescence modulation in the highly emissive dicyanodistyrylbenzene crystal: secondary bonding interaction in molecular stacking assembly*J. Mater. Chem.* **2011**;*21*:8338–8346. DOI: 10.1039/C0JM03711G

[13] Yang J, Ren Z, Chen B, Fang M, Zhao Z, Tang BZ, Peng Q, Li Z. Three polymorphs of one luminogen: how the molecular packing affects the RTP and AIE properties? *J. Mater. Chem. C* **2017**;*5*:9242–9246. DOI:1 0.1039/C7TC03656F

[14] Pick A, Klues M, Rinn A, Harms K, Chatterjee S, Witte G. Polymorph-Selective Preparation and Structural Characterization of Perylene Single Crystals. *Cryst. Growth Des.* **2015**;*15*:5495−5504. DOI: 10.1021/acs.cgd.5b01130

[15] Mallia AR, Sethy R, Bhat V, Hariharan M. Crystallization induced enhanced emission in conformational polymorphs of a rotationally flexible molecule. *J. Mater. Chem. C,* **2016**;*4*:2931–2935. DOI: 10.1039/C5TC03188E

[16] Gu X, Yao J, Zhang G, Yan Y, Zhang C, Peng Q, Liao Q, Wu Y, Xu Z, Zhao Y, Fu H, Zhang D. Polymorphism-Dependent Emission for Di(p-methoxylphenyl)dibenzofulvene and Analogues: Optical Waveguide/Amplified Spontaneous Emission Behaviors. *Adv. Funct. Mater.* **2012**;*22*;4862–4872. DOI: 10.1002/adfm.201201482

[17] Zhan Y, Wang Y. Donor-acceptor π-conjugated quinoxaline derivatives exhibiting multi-stimuli-responsive behaviors and polymorphism-dependent multicolor solid-state emission. *Dyes Pigm.* **2020**;*173*:107971. DOI: 10.1016/j.dyepig.2019.107971

[18] Sarkar SK, Pegu M, Behera SK, Narra SK, Thilagar P. Aggregation-Induced and Polymorphism-Dependent Thermally Activated Delayed Fluorescence (TADF) Characteristics of an Oligothiophene: Applications in Time-Dependent Live Cell Multicolour Imaging. *Chem. Asian J.* **2019**;*14*:4588–4593. DOI: 10.1002/asia.201901138

[19] Huang B, Chen W-C, Li Z, Zhang J, Zhao W, Feng Y, Tang BZ, Lee CS. Manipulation of Molecular Aggregation States to Realize Polymorphism, AIE, MCL, and TADF in a Single Molecule. *Angew. Chem. Int. Ed.* **2018**;*57*:12473–12477. DIO: 10.1002/anie.201806800

[20] Mutai T, Satou H, Araki K. Reproducible on-off switching of solid-state luminescence by controlling molecular packing through heat-mode interconversion. *Nature Mater.* **2005**;*4*:685–687. DOI: 10.1038/nmat1454

[21] Liu H, Lu Z, Ye K, Zhang Z, Zhang H. Polymorph-Dependent Luminescence Response to Acid Vapors and Its Application in Safety Protection of File Information. *ACS Appl. Mater. Interfaces* **2019**;*11*:34526–34531. DOI: 10.1021/acsami.9b14474

[22] Shida T, Mutai T, Araki K. Sterically induced polymorphism: ON–OFF control of excited-state intramolecular proton transfer (ESIPT) luminescence of 1-methyl-2-(2′-

hydroxyphenyl)benzimidazole. *CrystEngComm* **2013**;*15*:10179–10182. DOI: 10.1039/C3CE41742E

[23] Borbone F, Tuzi A, Panunzi B, Piotto S, Concilio S, Shikler R, Nabha S, Centore R. On–Off Mechano-responsive Switching of ESIPT Luminescence in Polymorphic N-Salicylidene-4-amino-2-methylbenzotriazole. *Cryst. Growth Des.* **2017**;*17*:5517–5523. DOI: 10.1021/acs.cgd.7b01047

[24] Devi K, Sarma RJ. Mechano-responsive luminescent emissions of an organic molecular crystal: effects of aromatic stacking interactions and solid state packing. *CrystEngComm* **2019**;*21*:4811–4819. DOI: 10.1039/C9CE00659A

[25] Yoshida A, Ikeshita M, Komiya N, Naota T. Solid-state fluorescence of zwitterionic imidazolium pyridinolates bearing long alkyl chains: Control of emission properties based on variation of lamellar alignment. *Tetrahedron* **2017**;*73*:6000–6007. DOI: 10.1016/j.tet.2017.08.045

[26] Tchoń D, Trzybiński D, Wrona-Piotrowicz A, Makal A. Polymorphism and resulting luminescence properties of 1-acetylpyrene. *CrystEngComm* **2019**;*21*: 5845–5852. DOI: 10.1039/C9CE01203F

[27] Ghodbane A, Fellows WB, Bright J, Ghosh D, Saffon N, Tolbert LM, Fery-Forgues S, Solntsev KM. Effects of the benzoxazole group on green fluorescent protein chromophore crystal structure and solid state photophysics. *J. Mater. Chem. C* **2016**;*14*:2793–2801. DOI: 10.1039/C5TC03776J

[28] Carayon C, Ghodbane A, Gibot L, Dumur R, Wang J, Saffon N, Rols MP, Solntsev KM, Fery-Forgues S. Conjugates of Benzoxazole and GFP Chromophore with Aggregation-Induced Enhanced Emission: Influence of the Chain Length on the Formation of Particles and on the Dye Uptake by Living Cells. *Small* **2016**;*12*:6602–6612. DOI: 10.1002/smll.201602799

[29] Carayon C, Fery-Forgues S. 2-Phenylbenzoxazole derivatives: a family of robust emitters of solid-state fluorescence. *Photochem. Photobiol. Sci.* **2017**;*16*:1020−1035. https://doi.org/10.1039/C7PP00112F

[30] Walker CL, Lukyanov KA, Yampolsky IV, Mishin AS, Bommarius AS, Duraj-Thatte AM, Azizi B, Tolbert LM, Solntsev KM. Fluorescence imaging using synthetic GFP chromophores. *Curr. Opin. Chem. Biol.* **2015**;*27*:64–74. DOI: 10.1016/j.cbpa.2015.06.002

[31] Mei J, Leung NLC, Kwok RTK, Lam JWY, Tang BZ. Aggregation-Induced Emission: Together We Shine, United We Soar! *Chem. Rev.* **2015**;*115*:11718–11940. DOI: 10.1021/acs.chemrev.5b00263

[32] De Mello JC, Wittmann HF, Friend RH. An improved experimental determination of external photoluminescence quantum efficiency. *Adv. Mater.* **1997**;*9*:230–232. DOI: 10.1002/adma.19970090308

[33] Sheldrick GM. SHELXT – Integrated space-group and crystal-structure determination. *Acta Cryst. A* **2015**;*71*:3–8. DOI: 10.1107/S2053273314026370

[34] Sheldrick GM. Crystal structure refinement with SHELXL. *Acta Cryst. C* **2015**;*71*:3–8. DOI : 10.1107/S2053229614024218

[35] Macrae CF, Edgington PR, McCabe P, Pidcock E, Shields GP, Taylor R, Towler M, van de Streek J. Mercury: visualization and analysis of crystal structures. *J. Appl. Cryst.* **2006**;*39*:453–457. DOI: 10.1107/S002188980600731X

[36] Becke AD. Density-functional thermochemistry. III. The role of exact exchange. *J. Chem. Phys.* **1993**;*98*:5648–5652. DOI: 10.1063/1.464913

[37] Andersson MP, Udval P. New Scale Factors for Harmonic Vibrational Frequencies Using the B3LYP Density Functional Method with the Triple-ζ Basis Set 6-311+G(d,p). *J. Phys. Chem. A* **2005**;*109*:2937–2941. DOI: 10.1021/jp045733a

[38] Adamo C, Barone V. Toward reliable density functional methods without adjustable parameters: The PBE0 model. *J. Chem. Phys.* **1999**;*110*:6158–6170. DOI: 10.1063/1.478522

[39] Becke AD. A new mixing of Hartree–Fock and local density-functional theories. *J. Chem. Phys.* **1993**;*98*:1372–1377. DOI: 10.1063/1.464304

[40] Bernardi F, Olivucci M, Robb MA. Potential energy surface crossings in organic photochemistry. *Chem. Soc. Rev.* **1996**;*25*:321–328. DOI: 10.1039/CS9962500321

[41] Frisch MJ, Trucks GW, Schlegel HB, Scuseria GE, Robb MA, Cheeseman JR, Scalmani G, Barone V, Petersson GA, Nakatsuji H, Li X, Caricato M, Marenich AV, Bloino J, Janesko BG, Gomperts R, Mennucci B, Hratchian HP, Ortiz JV, Izmaylov AF, Sonnenberg JL, Williams-Young D, Ding F, Lipparini F, Egidi F, Goings J, Peng B, Petrone A, Henderson T, Ranasinghe D, Zakrzewski VG, Gao J, Rega N, Zheng G, Liang W, Hada M, Ehara M, Toyota K, Fukuda R, Hasegawa J, Ishida M, Nakajima T, Honda Y, Kitao O, Nakai H, Vreven T, Throssell K, Montgomery JA Jr., Peralta JE, Ogliaro F, Bearpark MJ, Heyd JJ, Brothers EN, Kudin KN, Staroverov VN, Keith TA, Kobayashi R, Normand J, Raghavachari K, Rendell AP, Burant JC, Iyengar SS,

Tomasi J, Cossi M, Millam JM, Klene M, Adamo C, Cammi R, Ochterski JW, Martin RL, Morokuma K, Farkas O, Foresman JB, Fox DJ. Gaussian 16, Revision B.01. Gaussian, Inc., Wallingford CT, **2016**.

[42] Barca GMJ, Bertoni C, Carrington L, Datta D, De Silva N, Deustua JE, Fedorov DG, Gour JR, Gunina AO, Guidez E, Harville T, Irle S, Ivanic J, Kowalski K, Leang SS, Li H, Li W, Lutz JJ, Magoulas I, Mato J, Mironov V, Nakata H, Pham BQ, Piecuch P, Poole D, Pruitt SR, Rendell AP, Roskop LB, Ruedenberg K, Sattasathuchana T, Schmidt MW, Shen J, Slipchenko L, Sosonkina M, Sundriyal V, Tiwari A, G. Vallejo JL, Westheimer B, Wloch M, Xu P, Zahariev F, Gordon MS. Recent developments in the general atomic and molecular electronic structure system. *J. Chem. Phys.* **2020**;*152*:154102. DOI: 10.1063/5.0005188

[43] Shi J, Aguilar Suarez LE, Yoon S-J, Varghese S, Serpa C, Park SY, Lüer, D. Roca-Sanjuán D, Milián-Medina B, Gierschner J. Solid State Luminescence Enhancement in π-Conjugated Materials: Unraveling the Mechanism beyond the Framework of AIE/AIEE. *J. Phys. Chem. C* **2017**;*121*:23166–23183. DOI: 10.1021/acs.jpcc.7b08060

[44] Crespo-Otero R, Li Q, Blancafort L. Exploring Potential Energy Surfaces for Aggregation-Induced Emission—From Solution to Crystal. *Chem. Asian J.* **2019**;*14*:700–714. DOI: 10.1002/asia.201801649

[45] Nikiforov A, Gamez JA, Thiel W, Huix-Rotllant M, Filatov M. Assessment of approximate computational methods for conical intersections and branching plane vectors in organic molecules. *J. Chem. Phys.* **2014**;*141*:124122. DOI: 10.1063/1.4896372

[46] Polyakov IV, Grigorenko BL, Epifanovsky EM, Krylov AI, Nemukhin AV. Potential Energy Landscape of the Electronic States of the GFP Chromophore in Different Protonation Forms: Electronic Transition Energies and Conical Intersections. *J. Chem. Theory Comput.* **2010**;*6*:2377–2387. DOI: 10.1021/ct100227k

[47] Carayon C, Ghodbane A, Leygue N, Wang J, Saffon-Merceron N, Brown R, Fery-Forgues S. Mechanofluorochromic Properties of an AIEE-Active 2-Phenylbenzoxazole Derivative: More than Meets the Eye? *ChemPhotoChem* **2019**;*3*:545−553. DOI: 10.1002/cptc.201800261

[48] Majumdar P, Tharammal F, Gierschner J, Varghese S. Tuning Solid-State Luminescence in Conjugated Organic Materials: Control of Excitonic and Excimeric

Contributions through π Stacking and Halogen Bond Driven Self-Assembly. *ChemPhysChem* **2020**;*21*:616 –624. DOI: 10.1002/cphc.201901223

[49] Gierschner J, Ehni M, Egelhaaf HJ, Milián Medina B, Beljonne D, Benmansour H, Bazan C. Solid-state optical properties of linear polyconjugated molecules: π-stack contra herringbone. *J. Chem. Phys*. **2005**;*123*:144914. DOI: 10.1063/1.2062028

[50] Presti D, Wilbraham L, Targa C, Labat F, Pedone A, Menziani MC, Ciofini I, Adamo C. Understanding Aggregation-Induced Emission in Molecular Crystals: Insights from Theory. *J. Phys. Chem. C* **2017**;*121*:5747–5752. DOI: 10.1021/acs.jpcc.7b00488

[51] Dunitz JD, Bernstein J. Disappearing Polymorphs. *Acc. Chem. Res.* **1995**;*28*:193−200. DOI: 10.1021/ar00052a005

[52] Naito H, Nishino K, Morisaki Y, Tanaka K, Chujo Y. Highly-efficient solid-state emissions of anthracene–o-carborane dyads with various substituents and their thermochromic luminescence properties. *J. Mater. Chem. C* **2017**;*5*:10047–10054. DOI: 10.1039/C7TC02682J

[53] Wu X, Guo J, Jia W, Zhao J, Jia D, Shan H. Highly-efficient solid-state emission of tethered anthracene-o-carborane dyads and their visco- and thermo-chromic luminescence properties. *Dyes Pigm.* **2019**;*162*:855–862. DOI: 10.1016/j.dyepig.2018.11.018

[54] Ohtani S, Gon M, Tanaka K, Chujo Y. A Flexible, Fused, Azomethine–Boron Complex: Thermochromic Luminescence and Thermosalient Behavior in Structural Transitions between Crystalline Polymorphs. *Chem. Eur. J.* **2017**;*23*:11827–11833. DOI: 10.1002/chem.201702309

[55] Wei R, Song P, Tong A. Reversible Thermochromism of Aggregation-Induced Emission-Active Benzophenone Azine Based on Polymorph-Dependent Excited-State Intramolecular Proton Transfer Fluorescence. *J. Phys. Chem. C* **2013**;*117*:3467−3474. DOI: 10.1021/jp311020w

[56] Wu X, Guo J, Zhao J, Che Y, Jia D, Chen Y. Multifunctional luminescent molecules of o-carborane-pyrene dyad/triad: flexible synthesis and study of the photophysical properties. *Dyes Pigm*. **2018**;*154*:44–51. DOI: 10.1016/j.dyepig.2018.02.035

[57] Železný V, Jastrabík L, Dobiášová L. The Temperature Dependence of Emission Spectra in α-9, 10-Dichloroanthracene. *Phys. Stat. Sol. B* **1983**;*117*:K95–K97. DOI: 10.1002/pssb.2221170248

[58] Rivera M, Dommett M, Crespo-Otero R. Fromage: A Library for the Study of Molecular Crystal Excited States at the Aggregate Scale. *J. Chem. Theory Comput.* **2019**;*15*:2504–2516. DOI: 10.26434/chemrxiv.9786041.v1

[59] Pei K, Zhou H, Yin Y, Zhang G, Pan W, Zhang Q, Guo H. Highly fluorescence emissive 5, 5′-distyryl-3, 3′-bithiophenes: Synthesis, crystal structure, optoelectronic and thermal properties. *Dyes Pigm.* **2020**;*179*:108396. DOI: 10.1016/j.dyepig.2020.108396

[60] Hariharan PS, Gayathri P, Moon D, Anthony SP. Tunable and Switchable Solid State Fluorescence: Alkyl Chain Length-Dependent Molecular Conformation and Self-Reversible Thermochromism. *ChemistrySelect* **2017**;*2*:7799–7807. DOI: 10.1002/slct.201701550

[61] Schweikart KH, Hohloch M, Steinhuber E, Hanack M, Lüer L, Gierschner J, Egelhaaf H-J, Oelkrug D. Highly luminescent oligo(phenylenevinylene) films: The stereochemical approach. *Synth. Met.* **2001**;*121*:1641−1642. DOI: 10.1016/S0379-6779(00)00765-7

[62] Gierschner J, Lüer L, Milián-Medina B, Oelkrug D, Egelhaaf H-J. Highly Emissive H-Aggregates or Aggregation-Induced Emission Quenching? The Photophysics of All-Trans para-Distyrylbenzene. *J. Phys. Chem. Lett.* **2013**;*4*:2686−2697. DOI: 10.1021/jz400985t

[63] Dimitriev OP, Piryatinski YP, Slominskii YL. Excimer Emission in J-Aggregates. *J. Phys. Chem. Lett.* **2018**;*9*: 2138−2143. DOI: 10.1021/acs.jpclett.8b00481

[64] Saccone M, Blanke M, Daniliuc CG, Rekola H, Stelzer J, Priimagi A, Voskuhl J, Giese M. Mesogens with Aggregation-Induced Emission Formed by Hydrogen Bonding. *ACS Mater. Lett.* **2019**;*1*:589–593. DOI: 10.1021/acsmaterialslett.9b00371

[65] Wang Y, Chen Y, Huang Y, Zhang Q, Zhang Y, Li J, Jia C. A switch-on fluorophore using water molecules via hydrogen bonding and its application for bio-imaging of formaldehyde in living cells. *Anal. Meth.* **2019**;*11*:2311–2319. DOI:10.1039/C9AY00281B

[66] Wang M, Cheng C, Song J, Wang J, Zhou X, Xiang H, Liu J. Multiple Hydrogen Bonds Promoted ESIPT and AIE-active Chiral Salicylaldehyde Hydrazide. *Chin. J. Chem.* **2018**;*36*:698–707. DOI: 10.1002/cjoc.201800115

[67] Zhang G, Sun J, Xue P, Zhang Z, Gong P, Peng J, Lu R. Phenothiazine modified triphenylacrylonitrile derivates: AIE and mechanochromism tuned by molecular conformation. *J. Mater. Chem. C* **2015**;*3*:2925–2932. DOI: 10.1039/C4TC02925A

[68] Bremond E, Leygue N, Jaouhari T, Saffon-Merceron N, Erriguible A, Fery-Forgues S. Effect of substitution on the solid-state fluorescence properties of styrylbenzoxazole derivatives with terminal dicyanomethylene group. *J. Photochem. Photobiol. A* **2021**;*404*:112857. DOI: 10.1016/j.jphotochem.2020.112857